Tribol Lett (2011) 42:203–213
DOI 10.1007/s11249-011-9764-z

ORIGINAL PAPER

Environmental Effects on the Tribology and Microstructure of MoS_2–Sb_2O_3–C Films

Gregory J. Dudder · Xueying Zhao · Brandon Krick · W. Gregory Sawyer · Scott S. Perry

Received: 11 October 2010 / Accepted: 23 February 2011 / Published online: 19 March 2011

Abstract The tribology of molybdenum disulfide (MoS_2)–Sb_2O_3–C films was tested under a variety of environmental conditions (ambient 50% RH, 10^{-7} Torr vacuum, 150 Torr oxygen, and 8 Torr water) and correlated with the composition of the surface composition expressed while sliding. High friction and low friction modes of behavior were detected. The lowest coefficient of friction, 0.06, was achieved under vacuum, while sliding in 8 Torr water and ambient conditions both yielded the highest value of 0.15. Water vapor was determined to be the environmental species responsible for high friction performance. XPS evaluations revealed a preferential expression of MoS_2 at the surface of wear tracks produced under vacuum and an increase in Sb_2O_3 concentration in wear tracks produced in ambient air (50% RH). In addition, wear tracks produced by sliding in vacuum exhibited the lowest surface roughness as compared to those produced in other environments, consistent with the picture of low friction originating from well-ordered MoS_2 layers produced through sliding in vacuum.

Keywords Molybdenum disulfide · Antimony trioxide · Carbon tribology · Environmental dependence · XPS · AFM

1 Introduction

As an essential component to the deployment and operation of increasingly complex space apparati, solid lubricants are constantly asked to deliver reliable, low friction performance over a variety of environmental conditions [1, 2]. Molybdenum disulfide (MoS_2) is a common industrial solid lubricant with a layered crystal structure that has been relied upon for many decades [3, 4]. The drawback of using MoS_2 is its sensitivity to environmental conditions [5–7]. Operation under ambient, humid conditions has been found to lead to high friction, wear, and premature failure [8]. In the past, materials such as gold [9, 10], titanium [11], lead [12], carbon [13–15] tungsten diselenide (WSe_2) [16], and antimony trioxide (Sb_2O_3) [17, 18] have been evaluated as additives in an effort to address this problem.

Molybdenum disulfide was tested as a solid lubricant in the early 1940s with work continuing into the following decades aimed at explaining its inherent low friction behavior, the source of environmentally driven high friction, and substrate optimization [19–24]. The 1980s and 1990s saw an explosion of research into additives for MoS_2, their effectiveness, and the theory of their functions.

Given that the thickness of the active interface lies on the atomic scale, many studies have utilized surface sensitive techniques to effectively probe the nature of the interface. Auger electron spectroscopy (AES), X-ray photoelectron spectroscopy (XPS), scanning tunneling microscopy (STM), and atomic force microscopy (AFM) have been employed in tribological studies [12, 25–30]. AES and XPS played integral parts in determining the role of oxygen chemistry with MoS_2-based films. Operation in ambient and humid conditions was found to lead to the formation of MoO_3 within the wear track [8, 31–35]. STM and AFM data guided the development of theories related to defect site formation and detailed the frictional dependence of MoS_2 orientation [28, 36]. When used in conjunction with bulk characterization techniques such as X-ray diffraction (XRD) and scanning electron microscopy

G. J. Dudder · X. Zhao · B. Krick · W. G. Sawyer · S. S. Perry (✉)
University of Florida, Gainesville, USA
e-mail: ssp@ufl.edu

(SEM), the increased performance of the additives was theorized to be caused by a multitude of mechanisms: preferential reorientation of the active lubricant [37–39], densification of the microstructure [10, 17, 40], increased mechanical hardness [16, 40, 41], reduction of oxidation of molybdenum by sacrificial metal elements [42], passivation of edge-oriented grains [16, 43], and restriction of crack propagation, localized delamination [15, 39]. Simultaneously, gains were also achieved in the field of film synthesis and processing. Sputter deposition techniques allowed for the ability to control and optimize film density, orientation, architecture, layer thickness, grain size, and surface roughness. As a result, some of the best engineered coatings displayed remarkable operation in air as well as vacuum, as compared to the prior limited performance of pure MoS_2 [44–47].

In the last decade, the focus of solid lubricant design expanded to the development of adaptive films to provide low friction across a wider range of operating conditions as well as cyclical applications between different extreme environments. This goal was pursued through the incorporation of a second lubricating constituent, creating ternary, even quaternary component films [1, 44, 48–53]. MoS_2–Sb_2O_3–C is such an adaptive coating, combining the proven vacuum tribological performance of MoS_2 with graphitic carbon, commonly used for ambient, lubrication applications [54, 55]. While there are only a few reports on this particular class of coating, they are generally thought to function by preferential constituent migration toward the active interface with the top constituent becoming the primary lubricant. Secondary migration has also been observed and is thought to play a mechanical role supporting the active lubricant layer and providing a barrier to crack propagation, which can lead to wear and premature failure.

Prior reports of the tribology of MoS_2–Sb_2O_3–C coatings are extremely limited [55, 56]. Zabinski et al. utilized Auger, Raman, and energy dispersive spectroscopy (EDS), SEM, and TEM to investigate the wear track of this coating produced under different environmental conditions. Tribological testing of the coatings demonstrated high friction for an ambient, humid environment, and low friction for both vacuum and dry nitrogen environments. Hamilton et al. have also demonstrated low friction, low wear performance for these same coatings under dry nitrogen conditions. The Zabinski study reported evidence that the constituents present in the wear track change depending upon the operating environment. MoS_2 was measured to be the main component of tracks worn in vacuum and dry nitrogen conditions. The wear track in air was dominated by graphitic carbon and Sb_2O_3 according to AES measurements. Raman spectroscopy measurements did not detect a Sb_2O_3 signal. Tunneling electron micrographs and EDS show carbon to be concentrated both at the tribological interface as well as surrounding the larger Sb_2O_3 particles immediately below the interface. Environmental cycling between dry nitrogen and ambient conditions yielded wear tracks with distinct Raman spectra. The evidence pointed toward MoS_2 acting as the primary lubricant in a dry nitrogen environment, while graphite was the tribologically active constituent in the humid and ambient environment. Sb_2O_3 was acknowledged as playing several critical roles: reorienting the active lubricating component, providing a mechanically hard surface to support and isolate a thin layer of the active lubricant, preventing crack growth, and serving as an oxidation barrier. It has also been shown to affect the microstructure of MoS_2-based films, reducing intercolumnar porosity [57].

While the authors correlate wear track constituents under ambient, dry nitrogen, and vacuum conditions, there is a lack of testing of an oxygen rich and water-free environment. Such an inclusion would isolate whether the presence of water molecules are solely responsible for the degraded performance of the films, or whether it is a combination effect of oxygen and water acting together in an ambient and humid environment which brings about expedited surface crack formation and coating failure. Crack initiation and development is also a general topic which remains to be completely described. Understanding the location and process of subsurface micro crack formation and growth would benefit the design of future coatings.

The objective of this study is to correlate tribological performance with environmental, chemical, and microstructural changes to advance the model of constituent migration to the active interface of MoS_2–Sb_2O_3–C under different environmental conditions. The study employs complementary characterization techniques, XPS and AFM, to investigate and quantify the performance of MoS_2–Sb_2O_3–C coatings and the precise chemical nature and microstructure of the wear track produced by sliding under controlled conditions. The coatings have been evaluated in 10^{-7} Torr vacuum, in the presence of ambient air (50% RH), and in the presence of the individual components of this ambient condition: 150 Torr oxygen, 8 Torr water. The studies were performed with a custom in vacuo pin-on-disk tribometer, located in an isolated environmental chamber and interfaced with a monochromatic XPS system, thus avoiding the contamination of wear surfaces between tribological and spectroscopic tests. The design of the tribometer was based upon a series of space tribometers used as part of the MISSE 7 platform [58]. Microscopic analysis conducted with AFM provided topographical, microstructural, and localized friction behavior information directly from the wear track.

2 Experimental

2.1 Samples

MoS_2–Sb_2O_3–C coatings, 4–5 μm in thickness, were deposited using a proprietary method onto (100) silicon and 316 stainless steel coupons by Tribologix Inc. of Dayton, Ohio. The coated substrates (14 × 10 mm) were directly mounted to Omicron platens, allowing for use within both the pin-on-disk tribometer and Omicron XPS.

2.2 Tribometry

All measurements were made using a compact pin-on-disk tribometer, housed in an environment chamber connected to the XPS system. Figure 1 illustrates the tribometer with a sample inserted during operation. The tribometer featured a rotating sample holder, which secured platens on which the MoS_2–Sb_2O_3–C coated substrates mounted; these platens could be easily removed from the sample holders and placed directly in the XPS without ever opening the environment to and poisoning the sample with laboratory air. This sample holder was attached directly to the spindle of a Maxon vacuum compatible motor with an 84:1 reducer gearbox. The "pin" was a 3.175-mm diameter ball made of 440C steel; a circular flat of approximately 1 mm in diameter was produced on the ball surface through polishing in situ by sliding on the required polishing media. This procedure had the effect of increasing the width of the wear track and the area available for subsequent analysis. This "pin" was cleaned but not removed after polishing to ensure proper alignment. It was held in place with a set screw in one end of a monolithic biaxial force transducer and loading flexure (or "flexure"). Upon introduction of coating samples, the alignment of the flattened pin was evaluated by operating the tribometer in both clockwise and counterclockwise rotations for ten cycles. The measured coefficient of friction values was evaluated and averaged for each direction and found to be within 0.004. The flexure was instrumented with two sets of strain gage in full Wheatstone bridge configurations; one set measured the normal force while another measured the tangential (friction) force. Loading was achieved using a piezo-electric actuator assembly which pulled downward on the flexure, pulling the pin in contact with the sample. Nominal operating parameters and environments for the tribology experiments are given in Table 1.

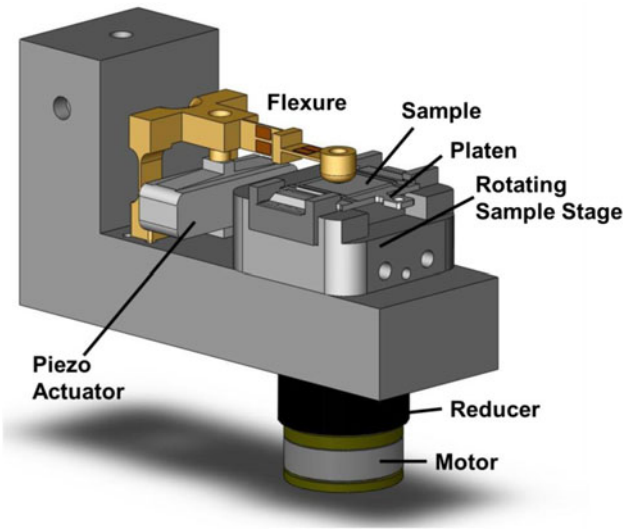

Fig. 1 Schematic illustration of the in vacuo pin-on-disk tribometer

Table 1 The parameters of pin-on-disk tests

Operating parameter	Value
Normal load	1.0 N
Disk rotation speed	5 rpm
Wear track diameter	7 mm
Linear sliding speed	1.9 mm/s
Nominal contact pressure	1.2 MPa
Temperature	25 °C
Environment	760 Torr air at 50% RH
	150 Torr oxygen
	8 Torr water
	10^{-7} Torr vacuum

For each environmental condition, three tests of at least 300 cycles were performed in neighboring locations on the same sample to generate a large wear area to ensure that the majority of XPS data collected corresponded to regions of wear. Although there existed as much as 100 μm between the wear tracks, the wear tracks composed approximately half of the analyzed area. The width of each wear tracks was measured to be at least 100 μm via a camera mounted above the AFM stage.

Normal and tangential force signals were collected every 50 ms; this data was averaged at 1 s interval and saved to a summary data file. The summary data was then averaged again at 12 s intervals to generate an average friction coefficient for each cycle; these were plotted as the average coefficient of friction per cycle in Fig. 2. The coefficient of friction reported for a specific environmental condition represents the average of cycles 100–300. Uncertainty in measured friction coefficient is better than 0.002, which is substantially less than the variation of the measured friction coefficient.

2.3 XPS

An Omicron Al K_α (1486.7 eV) monochromatic XPS source was used with an EAC2000-Sphera hemispherical,

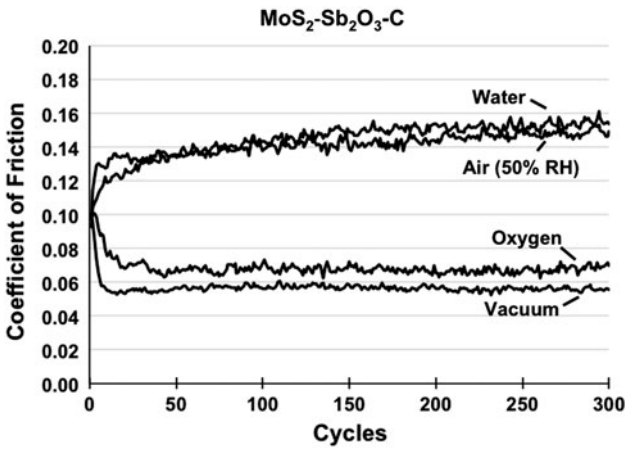

Fig. 2 Average coefficient of friction per rotation versus cycles for MoS_2–Sb_2O_3–C films run under 8 Torr water, 760 Torr air at 50% RH, 10^{-7} Torr vacuum, and 150 Torr oxygen

seven-channel analyzer. Calibrated with a 99.99% pure silver sample to measure a silver $3d_{5/2}$ peak at 368.30 eV, a circular aperture produced an electron collection area 700 μm in diameter. XPS spectra were collected using a step size of 0.05 eV and a pass energy of 20 eV from the molybdenum 3*d*, sulfur 2*p*, antimony 3*d*, oxygen 1*s*, and carbon 1*s* core regions. The antimony 3*d* and oxygen 1*s* core spectra occur within the same binding energy range and thus were measured together. Sensitivity factors for quantitative analysis were taken from the PHI XPS Handbook and assumed a 90° relationship between the incident X-rays and the electron analyzer [59]. 3*d* peak splits were fixed to a 3:2 real ratio and 2*p* peak splits were fixed to a 2:1 ratio. The fit of the oxygen intensity to a multiple of species was guided by stoichiometric relationships of the compound found to contain oxygen. The Mo 3*d* peak splits were fixed at 3.1 eV between the $3d_{5/2}$ and $3d_{3/2}$ components. S 2*p* peaks were fixed at 1.18 eV between the $2p_{3/2}$ and $2p_{1/2}$, while Sb 3*d* peak splits were fixed at 9.34 eV separation values according to the literature [59]. All peaks within a core region were constrained to the have the same FWHM value and were treated with a 90% Gaussian, 10% Lorentzian shape. A fitting algorithm, minimizing the squared sum of the difference between the artificial peaks and the measured spectrum, was used to finalize the overall peak fit spectrum. Fitting was complete when the value of the standard deviation of the residual spectrum was less than 2.0. For example, the standard deviation of 1.77 in Fig. 4a is comparable to an unfit area of 0.35 at% of the overall film composition.

2.4 AFM

An Asylum Research MFP-3D AFM was operated in a constant force contact mode, analyzing both the as-received films as well as wear tracks produced in air and vacuum. The Si_3N_4 cantilever was measured to have a normal stiffness of 0.61 N/m via thermal harmonic analysis, and the lateral force sensitivity was calculated using the wedge method [60]. Constituent size and distribution over the film surfaces were analyzed through lateral force detection. The lateral signals were converted to maps of the lateral force acting on the cantilever during translation across the coating surface. The mean friction forces were calculated by taking the difference between the trace and retrace signals and dividing by two. Constituents within the microstructure displayed distinctive coefficients of friction, allowing the delineation of one constituent from another.

3 Results

Tribological pin-on-disk testing revealed a strong initial environmental dependence for the MoS_2–Sb_2O_3–C films. Figure 2 displays coefficients of friction versus cycle for the four environmental conditions evaluated. In less than 50 cycles, trends were established for high and low friction regimes. Low friction was measured under oxygen and vacuum environments. The lowest coefficient of friction was measured in vacuum with a value of 0.06. High friction was measured under ambient and partial pressures of water with friction coefficients around 0.15. For both ambient and water conditions, the average coefficient per cycle increases immediately after the start of testing. Based on these results, water is identified as the species responsible for high friction behavior. The effect of the environment can also be noticed under vacuum and oxygen conditions, whereby the average coefficient decreases from the test initiation. Extended sliding for both ambient and vacuum conditions was conducted for over 5000 cycles for two environments (data not shown). The coefficient of friction for air remained constant and stable, while the coefficient of friction for the film in vacuum continued to decrease until reaching a steady state value less than 0.03.

Spectroscopic analysis of the films both on and off the wear tracks revealed the following chemical species portrayed in Fig. 3. For an unworn film, MoS_2 peaks were detected in the Mo 3*d* spectrum, Fig. 3a. They were identified at binding energies of 229.0 and 232.1 eV. Likewise, in Fig. 3b, the S 2*p* spectrum had resolvable peaks at 161.8 and 163.0 eV corresponding to MoS_2. Both the molybdenum and sulfur peaks agreed with established literature values for MoS_2 [25, 26, 33, 61]. Additional peaks evident in Fig. 3a at binding energies of 232.3 and 235.4 eV are assigned to MoO_3 [25, 33, 62]. A second sulfur species detected primarily on unworn surfaces was strongly exhibited in the vacuum sample. This species was identified as sulfate characterized by binding energies of

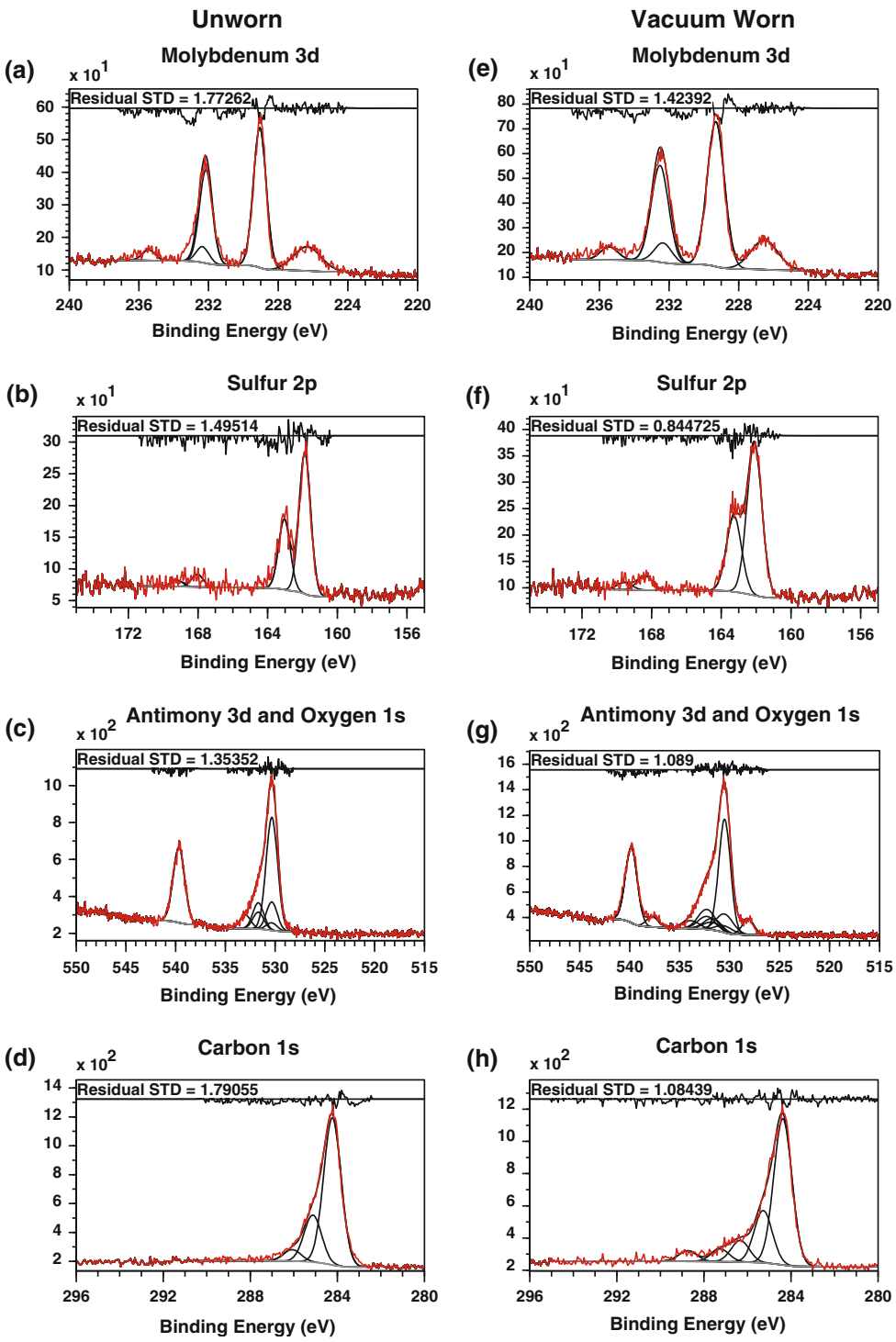

Fig. 3 X-ray photoelectron spectra of unworn MoS_2–Sb_2O_3–C **a** molybdenum 3*d* spectrum, **b** sulfur 2*p* spectrum, **c** antimony 3*d* and oxygen 1*s* spectra, and **d** carbon 1*s* spectrum and MoS_2–Sb_2O_3–C wear track under vacuum **e** molybdenum 3*d* spectrum, **f** sulfur 2*p* spectrum, **g** antimony 3*d* and oxygen 1*s* spectra, and **h** carbon 1*s* spectrum

168.7 and 169.9 eV. This correlated well with a strong O 1*s* signal at 532.3 eV having a corresponding 4:1 intensity ratio (Fig. 2c). The measured C 1*s* spectrum shown in Fig. 3d consisted of a majority of C–C bonding, as indicated by the intensity at 284.2 and 285.1 eV. The existence of two peaks was attributed to sp^2 and sp^3 hybridized bonding or edge defects (C–H bonding) [63, 64]. The absence of a corresponding feature at 291.0 eV suggested that the carbon present in the film had either minor long range graphitic order, or more likely was amorphous having no long range crystallinity [63, 65, 66]. The smallest peak at 286.0 eV was assigned to C–O bonding. Figure 3c shows the overlapping Sb 3*d* and O 1*s* spectra. In this convoluted region, Sb_2O_3 peaks resulting from the $3d_{5/2}$

and $3d_{3/2}$ of the antimony atom appear at 530.3 and 539.6 eV. The oxygen intensity arising from Sb_2O_3, as well from MoO_3, is assigned to a value of 530.3 eV. Although this is slightly higher than the 530.0 eV value often listed in literature [59, 67–70], it provides a consistent fit throughout the series of data sets. The O 1*s* intensity at a binding energy of 532.3 eV is attributed to C–O and SO_4 species [59, 71, 72], while intensity at 533.0 eV is assigned as arising from H_2O [72].

Many of the same features are observed in the spectra obtained from the wear track generated in a vacuum environment (Fig. 3e–h). In addition, the vacuum worn wear track was found to contain C=O and O–C=O bonding due to surface contamination, Fig. 3h. Here, C=O bonding is located at 287.6 eV while evidence for O–C=O species is observed at 288.8 eV. The O 1*s* spectrum was correspondingly fit (Fig. 3g) with two signals, one for O–C=O and the other for the O–C=O component. The O–C=O bond is expected to be at a higher binding energy than the O–C=O. Values of 533.9 eV for O–C=O and 531.7 eV for O–C=O have been reported in the literature. C=O bonding is assigned intensity at 531.7 eV [59, 71, 72]. Elsewhere for the vacuum worn surface, the only appreciable chemical alteration in constituent species appears in the reduction of antimony trioxide to metallic antimony. This species was detected only following tribological measurements under vacuum conditions. It is notable that the strength of this signal decreased with time after tribological testing was finished, indicating the reactivity of the species, even in vacuum. No other reactions or decomposition of the composite constituents were detected.

Further analysis of these data reveals the greatest compositional change upon wear in vacuum to be the increase in MoS_2 intensity, coinciding with a decrease in carbon intensity. This finding is borne out in surface concentrations, expressed in atomic percentages following normalization with relevant elemental sensitivity factors. The composition of the near surface region of the as-received film (Fig. 3a–d) is 67.3% graphitic carbon, 10.6% MoS_2, 7.3% Sb_2O_3, 8.1% C–O, 3.2% SO_4, 2.0% H_2O, and 1.5% MoO_3. The composition of the near surface region of the vacuum wear track is 47.5% graphitic carbon, 13.5% MoS_2, 8.0% Sb_2O_3, 24.1% C–O_x, 4.2% SO_4, 2.3% MoO_3, and 0.4% metallic Sb. Similar tribological measurements and spectroscopic analyses were performed on the resulting wear tracks generated under ambient (50% RH) environments and under partial pressures of oxygen and water (data not shown). The composition of the wear track in ambient operation was 61.9% graphite, 13.14% MoS_2, 11.1% Sb_2O_3, with 7.5% C–O, 3.0% SO_4, 1.8% MoO_3, and 1.5% H_2O. Initial differences between the wear track compositions of the ambient and vacuum wear tracks show the near surface regions of the ambient wear track to have a higher graphite and Sb_2O_3 content while vacuum wear tracks contain have more MoS_2.

The XPS characterization of the wear tracks generated under an oxygen partial pressure environment shows Mo 3*d* peak of MoS_2 located at 229.1 and 232.2 eV. Mo 3*d* peaks of MoO_3 peaks were at 232.3 and 235.4 eV. The S 2*p* spectrum has MoS_2 peaks at 162.0 and 163.1 eV. There is a slight signal attributed to an SO_4 species at 168.1 and 169.3 eV. The C 1*s* spectrum is comprised of three carbon species: C–C (284.3 eV), C–H (285.2 eV), and C–O (286.2 eV). The Sb 3*d* spectrum is assigned with intensity arising from Sb_2O_3 with peaks at 530.3 and 539.6 eV. These are the same values as those fit with the ambient sample. Finally, the O 1*s* spectrum was assigned as having contributions from Sb_2O_3 and MoO_3 peaks at 530.3 eV and C–O at 531.7 eV. The final composition for the oxygen wear track was calculated as 60.2% graphitic carbon, 16.9% MoS_2, 11.7% Sb_2O_3, 5.3% C–O, 3.0% MoO_3, and 3.0% SO_4. Tribological testing of the film in partial pressures of water resulted in spectral features similar to those observed above. Only differences in the relative presence of the different species present were observed. The computed quantitative composition for the water sample was 58.4% graphitic carbon, 16.3% MoS_2, 11.5% Sb_2O_3, 8.0% C–O, 2.2% MoO_3, 2.1% SO_4, and 1.5% H_2O. For the wear tracks generated in partial pressures of water and oxygen, a higher MoS_2 composition than the ambient wear track is detected in the near surface region. Table 2 provides a summary of the XPS fit peak data.

Microstructural characterization via AFM, Fig. 4, indicated that wear of the coating surface also produced a reduction in surface roughness for wear tracks in both air and vacuum. Roughness values measured as RMS over representative 2×2 μm areas were 18 nm for the as-received film, 9 nm for the wear track in air, and 6 nm for the wear track in vacuum. The as-received film surface expressed circular particles less than 100 nm in diameter, while the rest of the morphology was relatively smooth. A portion of the wear track resulting from operation in air is shown in Fig. 4b, with evidence of plowing seen in the streaking from left to right. Even with the existence of this topography, the roughness has been reduced to approximately half that of the as-received film, suggesting the tribological interaction flattens the composite microstructure even in the most severe of the environments tested. This effect is even more clearly evident in the image taken from the wear track in vacuum; Fig. 4c contains very few distinguishing features across the field of view—neither the low frequency of surface particles present in Fig. 4a nor the plowing scars in Fig. 4b are evident across the wear track produced in vacuum.

Table 2 Fit XPS peak binding energies

Species	Peak	Unworn	Air (50% RH)	Vacuum	Oxygen	Water
MoS_2	Mo $3d_{5/2}$	229.0	229.0	229.3	229.1	229.1
MoS_2	Mo $3d_{3/2}$	232.1	232.1	532.4	232.2	232.2
MoS_2	S $2p_{3/2}$	161.8	161.8	162.1	162.0	161.9
MoS_2	S $2p_{1/2}$	163.0	163.0	163.3	163.1	163.1
MoO_3	Mo $3d_{5/2}$	232.2	232.4	232.3	232.3	232.3
MoO_3	Mo $3d_{3/2}$	235.4	235.4	235.4	235.4	235.4
MoO_3	O 1*s*	530.3	530.3	530.5	530.3	530.3
Sb_2O_3	Sb $3d_{5/2}$	530.3	530.3	530.5	530.3	530.3
Sb_2O_3	Sb $3d_{3/2}$	539.6	539.6	539.8	539.6	539.7
Sb_2O_3	O 1*s*	530.3	530.3	530.5	530.3	530.3
C–C	C 1*s*	284.2	284.2	284.4	284.3	284.2
C–C	C 1*s*	285.1	285.1	285.3	285.2	285.1
C–O	C 1*s*	286.0	285.9	286.3	286.2	286.2
C–O	O 1*s*	532.3	531.7	532.2	531.7	531.7
C=O	C 1*s*	–	–	287.6	–	–
C=O	O 1*s*	–	–	531.7	–	–
O–C=O	C 1*s*	–	–	288.8	–	–
O–C=O	O 1*s*	–	–	533.9	–	–
O–C=O	O 1*s*	–	–	531.7	–	–
SO_4	S $2p_{3/2}$	168.7	168.1	168.4	168.1	–
SO_4	S $2p_{1/2}$	169.9	169.3	169.6	169.3	–
SO_4	O 1*s*	532.3	531.7	532.2	531.7	–
H_2O	O 1*s*	533.0	533.0	–	–	533.0

Underscore indicates origin of photoelectron

The corresponding lateral force images collected in the identical regions as the topography presented in Figs. 4a–c provide additional insight into the dynamic nature of the coating surface as a function of wear. Although all three friction images were collected in an ambient air environment, differences in the film character are still apparent. Dark regions indicate areas of low friction, whereas light regions represent higher friction. The brightness of these images has been adjusted to allow a direct comparison of the mean friction experienced during the sliding of the Si_3N_4 tip across the surface. Figure 4d displays the spatially resolved friction of the as-received film, revealing a localized contrast in intensity caused by the composite nature of the film. In Fig. 4e, measured from the wear track in air, the mean friction of the wear surface is clearly seen to be higher. In addition, friction is seen to be largely independent of the surface topography (plowing marks) and the size of the features exhibiting the highest friction increases. Figure 4f depicts the lateral force measured within the wear track generated by sliding under vacuum. Here, regions of low friction are prevalent and numerous compared to the wear track in air, with a general reduction in mean friction also observed.

4 Discussion

Together, the XPS and AFM results obtained from wear surfaces generated through tribological measurement performed under carefully controlled environmental conditions reflect specific changes in surface composition as a function of sliding environment. In order to more fully evaluate the effect of operating in different environmental conditions, ratios of the normalized XPS integrated intensities for each species were calculated for regions both within and outside of the wear track. The change in the ratios from the film to the wear track gives an analysis method for determining which species are prevalent in the film and which species preferentially remain within the wear track. The direct comparison of worn and unworn regions exposed to the same environmental conditions provides the opportunity to separate tribologically induced changes from those potentially occurring through adsorption and/or reaction. Figure 5 shows the change in the ratio of MoS_2:Sb_2O_3, MoS_2:C, S:C, and MoS_2:MoO_3 and Sb_2O_3:C for each environmental condition. The expressed uncertainty of the ratios represents the sum of errors in the spectral fits of the two species being compared.

In comparing the collection of ratios between the various environments, the greatest change in surface composition is seen to occur when sliding occurs under vacuum conditions, where MoS_2:C increases by more than 75%. Likewise, Sb_2O_3:C increases by more than 75% while the MoS_2:Sb_2O_3 ratio experiences a positive change, suggesting an overall migration of both MoS_2 and Sb_2O_3 during tribological interactions under vacuum, with MoS_2 being the most preferred. From this analysis, it can be concluded that the presence of MoS_2 heavily contributes to the low friction performance under vacuum. It is worth noting, however, that the carbon ratios could be influenced by removal of adventitious carbon from the surface during the initial sliding cycles.

For operation in ambient air, the picture is different. There is a strong decrease in the MoS_2:Sb_2O_3 ratio and an increase in the Sb_2O_3:C ratio. The positive MoS_2:C and S:C ratios may again be partially influenced by the removal of adventitious carbon during tribological testing. Given this, the XPS data suggests that the surface of the wear track in air is influenced by interactions involving Sb_2O_3. There is still a large percentage of the overall wear track composition that is carbon, 57%, but only Sb_2O_3 is observed to increase in prevalence at the surface under these conditions. This could be an additional source of the increase in friction measured both in macroscopic and microscopic measurements of the wear track surface. However, in a recent study of a similar composite system, Scharf et al. demonstrated that Sb_2O_3 islands within the wear track serve as a load support and reduce wear under

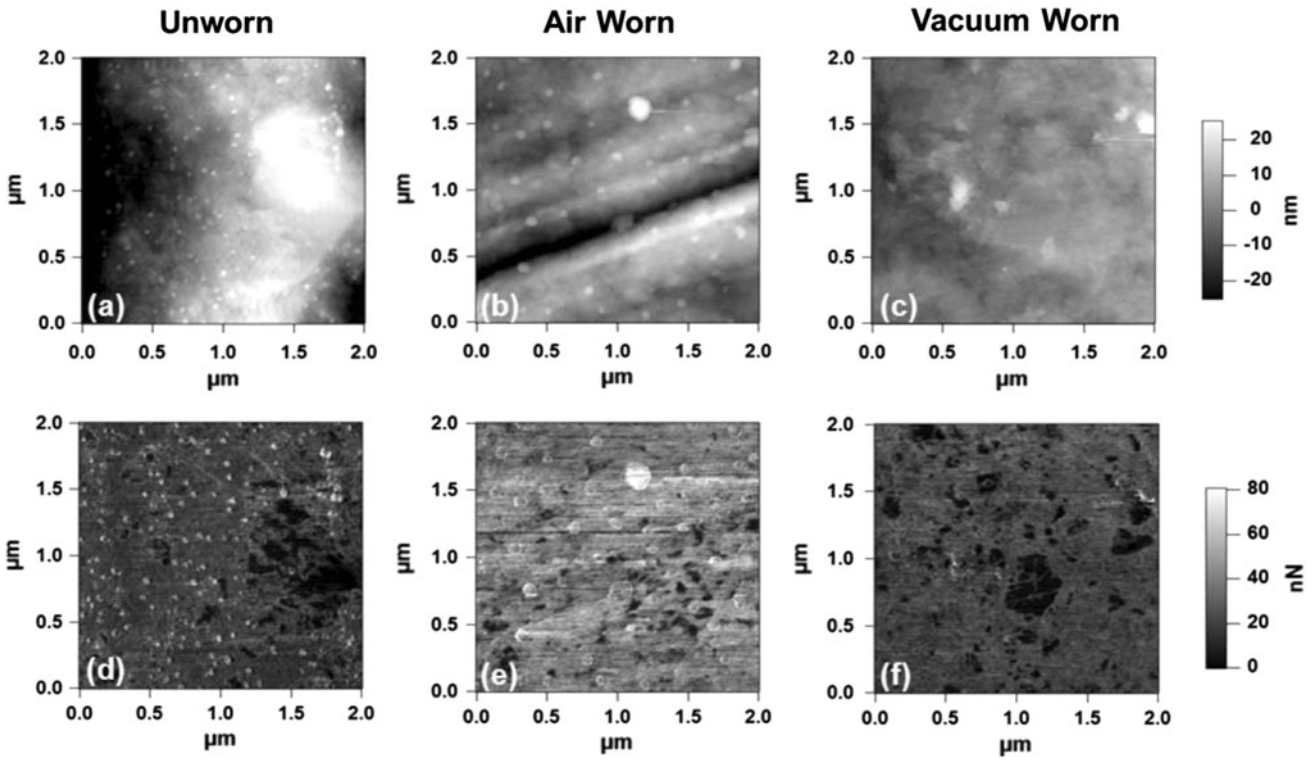

Fig. 4 Topographical maps of MoS_2–Sb_2O_3–C film **a** unworn film, **b** air 50% RH, and **c** 10^{-7} Torr vacuum and concurrent lateral force maps of MoS_2–Sb_2O_3–C film **d** unworn film, **e** air 50% RH, and **f** 10^{-7} Torr vacuum

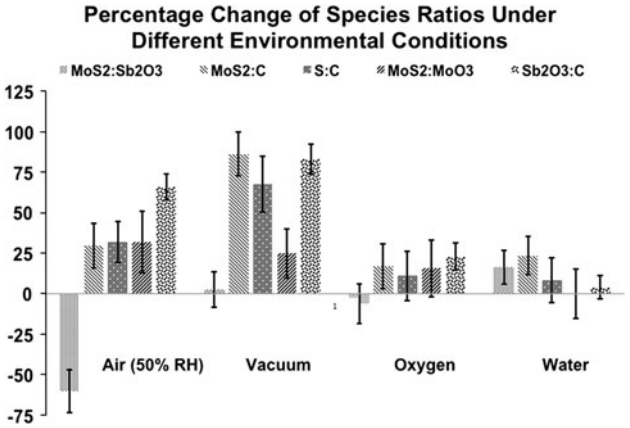

Fig. 5 The percentage change of the ratios of species as measured by XPS from off track to on track of each MoS_2–Sb_2O_3–C film run under, 760 Torr air at 50% RH, 10^{-7} Torr vacuum, 150 Torr oxygen, and 8 Torr water

humid conditions, highlighting the multifaceted role of some film components [57].

In comparing the changes observed in the other environments, the larger magnitude of the changes occurring under ambient conditions compared to those of oxygen and water conditions may indicate a synergistic wear process. Operation in oxygen seems to have very little effect on the surface composition with the most notable change occurring in the modest decrease of the MoS_2:MoO_3 ratio. This suggests that tribological interactions under this environment may be controlled by carbon species. Evaluation in partial pressures of water yields few similarities with air (50% RH), however, oxygen environmental testing does. For both air and oxygen conditions, the ratio of MoS_2:Sb_2O_3 decreases. This is coupled with an increase in the Sb_2O_3:C ratio. Concerning the oxidation of MoS_2, only water conditions produced a net decrease in the MoS_2:-MoO_3 ratio, suggesting that while the oxidation of MoS_2 is not strongly exhibited in these composite films, aqueous species are the most likely to bring about oxidation of the coating.

Friction, spectroscopic, and microscopic data are all crucial in describing the tribological interactions of MoS_2–Sb_2O_3–C in different environments. Pin-on-disk testing reinforces the sensitivity of MoS_2-based lubricants to water and suggests that it is the presence of water molecules and only water molecules that causes structural reorganization of the coating surface and is responsible for the higher friction behavior observed under ambient conditions. Spectroscopic data and lateral force maps present similar trends. The composite nature of the film is disrupted and species are presented at the surface to relieve the energetics at play. This newly formed surface can result from the

formation of a tribofilm or the generation of third bodies within the sliding interface and may signal a transition in the location of shear within the interface. While material transfer to the pin was not directly probed, the trends in Fig. 5 suggest that low friction performance of these interfaces is enabled by the enrichment of MoS_2 species within the interfacial tribofilm. This correlates with previous findings by Dvorak et al. that MoS_2-based films were found to contain mainly MoS_2 within the wear track and little evidence for oxidation within the wear track during ambient sliding [73]. For vacuum conditions, the dramatic increase in MoS_2:C provides evidence of MoS_2 being the primary lubricant at the surface controlling tribological behavior marked by low friction performance. A secondary constituent, Sb_2O_3 can also be detected as being at the surface via XPS. The increase in Sb_2O_3 in both vacuum and ambient conditions agrees with previous studies of MoS_2–Sb_2O_3, which identified Sb_2O_3 as a component acting synergistically with MoS_2. Previous testing of MoS_2–Sb_2O_3 films found enrichment of only MoS_2 at the surface of both the film and tip of the pin. However, TEM micrographs and Raman spectroscopy have indicated the location of Sb_2O_3 directly beneath the lubricating MoS_2 surface [39, 55].

Regarding the effect of operating in ambient conditions, XPS measurements show an increase of Sb_2O_3 at the expense of MoS_2 at the surface. Lateral force mapping indicates a change in surface constituents through an increase in friction. Topographical features do not appear to play a role in the increased friction due to the fact that the wear tracks are difficult to resolve in the lateral force map compared to the as-received film. Upon closer inspection of Fig. 4e, the smearing of particles, creating high friction regions in the direction of the sliding lends support to them being Sb_2O_3 as this correlates with the increase in Sb_2O_3:C seen in the XPS measurements. As stated earlier, carbon remains the majority constituent in the near surface region of the ambient wear track and its role in either controlling or moderating the friction and wear at the surface cannot be ruled out. However, the tribological data presents a clear role for water in MoS_2-based lubricants. The negative effects of operating in ambient conditions (high friction performance) can be directly related to the presence of an aqueous species in the atmosphere.

5 Conclusions

Composite, solid lubricant MoS_2–Sb_2O_3–C films exhibit an environmental dependence, which affects friction properties, surface composition, and microstructure within the wear track. In this study, two types of friction behavior have been identified. Testing in vacuum or partial pressures of oxygen environments yields a low friction behavior, while sliding in ambient (50% RH) conditions or partial pressures of water results in a high friction behavior. In this systematic study, water has been determined to be the species responsible for detrimental tribological performance. Importantly, partial pressures of oxygen are shown to have an inconsequential effect on the coefficient of friction with values remaining near the lowest obtained in vacuum. Sliding on these film surfaces under vacuum serves to preferentially bring MoS_2 to the surface, producing a low friction, exceedingly smooth wear track. Testing under ambient conditions produces a higher friction surface with increased Sb_2O_3 concentration and lowered MoS_2 composition. Evaluation of wear tracks produced by sliding in partial pressures of oxygen and water reveals only modest changes in near surface composition, yet a marked difference in tribological response, with high friction produced in the presence of water vapor, but not in the presence of molecular oxygen.

Acknowledgments This study was supported by an AFOSR grant FA9550-08-1-0027. Any opinions, findings, conclusions, or recommendations expressed in this material are those of the authors and do not necessarily reflect the views of the Air Force Office of Scientific Research.

References

1. Muratore, C., Voevodin, A.A.: Chameleon coatings: adaptive surfaces to reduce friction and wear in extreme environments. Annu. Rev. Mater. Sci. **39**, 297–324 (2009)
2. Hilton, M.R., Fleischauer, P.D.: Applications of solid lubricant films in spacecraft. Surf. Coat. Technol. **54**(55), 435–441 (1992)
3. Dickinson, R.G., Pauling, L.: The crystal structure of molybdenite. J. Am. Chem. Soc. **45**, 1466–1471 (1923)
4. Winer, W.O.: Molybdenum disulfide as a lubricant: a fundamental review of the fundamental knowledge. Wear **10**, 422–452 (1967)
5. Peterson, M.B., Johnson, R.L.: Friction and wear investigations of molybdenum disulfide I: effect of moisture. NACA Technical Note 3055(1953)
6. Bolster, R.N., Singer, I.L., Wegand, J.C., Fayuelle, S., Gossett, C.R.: Preparation by ion-beam-assisted deposition, analysis and tribological behavior of MoS_2 films. Surf. Coat. Technol. **46**, 207–216 (1991)
7. Ohmae, N.: Humidity effects on tribology of advanced carbon materials. Tribol. Int. **39**, 1497–1502 (2006)
8. Martin, J.M., Pascal, H., Donnet, C., Le Mogne, T., Loubet, J.L., Epicier, T.: Superlubricity of MoS_2: crystal orientation mechanisms. Surf. Coat. Technol. **68–69**, 427–432 (1994)
9. Stupp, B.C.: Synergistic effects of metals co-sputtered with MoS_2. Thin Solid Films **84**, 257–266 (1981)
10. Spalvins, T.: Frictional and morphological properties of Au–MoS_2 films sputtered from a compact target. Thin Solid Films **118**, 375–384 (1984)
11. Teer, D.G., Hampshire, J., Fox, V., Bellido-Gonzalez, V.: The tribological properties of MoS_2/metal composite coatings deposited by closed field magnetron sputtering. Surf. Coat. Technol. **94**, 572–577 (1997)

12. Wahl, K.J., Seitzman, L.E., Bolster, R.N., Singer, I.L.: Low-friction, high-endurance, ion-beam-deposited Pb–Mo–S coatings. Surf. Coat. Technol. **73**, 152–159 (1995)
13. Devine, M.J., Lamson, E.R., Bowen, J.H.: Inorganic solid film lubricants. J. Chem. Eng. Data. **6**, 79–82 (1961)
14. Hopkins, V., Gaddis, D.: Friction of solid film lubricants being developed for use in space environments. Lubr. Eng. **21**, 52–58 (1965)
15. Gardos, M.N.: The synergistic effects of graphite on the friction and wear of MoS_2 films in air. Tribol. Trans. **31**, 214–227 (1988)
16. Simmonds, M.C., Savan, A., Pflüger, E., Van Swygenhoven, H.: Mechanical and tribological performance of MoS_2 co-sputtered composites. Surf. Coat. Technol. **126**, 15–24 (2000)
17. Centers, P.W.: The role of oxide and sulfide additions in solid lubricant compacts. Tribol. Trans. **31**, 149–156 (1987)
18. Zabinski, J.S., Donley, M.S., McDevitt, N.T.: Mechanistic study of the synergism between Sb_2O_3 and MoS_2 lubricant systems using Raman spectroscopy. Wear **165**, 103–108 (1993)
19. Bell, M.E., Findlay, J.H.: Molybdenite as a new lubricant. Phys. Rev. **59**, 922 (1941)
20. Boyd, J., Robertson, B.P.: The friction properties of various lubricants at high pressures. ASME Trans. **67**, 51–59 (1945)
21. Deacon, R.F., Goodman, J.F.: Lubrication by lamellar solids. Proc. R Soc. London Ser. A. **243**, 464–482 (1958)
22. Salomon, G., De Gee, A.W.J., Zaat, J.H.: Mechano-chemical factors in MoS_2-film lubrication. Wear **7**, 87–101 (1964)
23. Brainard, W.A.: The thermal stability and friction of the disulfides, diselenides, and ditellurides of molybdenum and tungsten in vacuum (10^{-9} to 10^{-6} Torr). NASA, Washington, DC (1969)
24. Stupian, G.W.: Adhesion of MoS_2 powder burnished on metal substrates. J. Vac. Sci. Technol. **13**, 684–692 (1976)
25. Lince, J.R., Frantz, P.P.: Anisotropic oxidation of MoS_2 crystallites studied by angle-resolved X-ray photoelectron spectroscopy. Tribol. Lett. **9**, 211–218 (2000)
26. Savan, A., Simmonds, M.C., Huang, Y., Constable, C.P., Creasey, S., Gerbig, Y., Haefke, H., Lewis, D.B.: Effects of temperature on the chemistry and tribology of co-sputtered MoS_{2x}–Ti composite thin films. Thin Solid Films **489**, 137–144 (2005)
27. Le Mogne, T., Donnet, C., Martin, J.M., Tonck, A., Millard-Pinard, N., Fayuelle, S., Moncoffre, N.: Nature of super-lubricating MoS_2 physical vapor deposition coatings. J. Vac. Sci. Technol. A **12**, 1998–2004 (1993)
28. Zhang, X., Celis, J.P.: Nanotribology of MoS_x coatings investigated by oscillating lateral force micoscopy. Appl. Surf. Sci. **206**, 110–118 (2003)
29. Zabinski, J.S., Donley, M.S., Dyhouse, V.J., McDevitt, N.T.: Chemical and tribological characterization of PbO–MoS_2 films grown by pulsed laser deposition. Thin Solid Films **214**, 156–163 (1992)
30. Lince, J.R.: Tribology of co-sputtered nanocomposite Au/MoS_2 solid lubricant films over a wide contact stress range. Tribol. Lett. **17**, 419–428 (2004)
31. Lince, J.R.: $MoS_{2-x}O_x$ solid solutions in thin films produced by rf-sputter-deposition. J. Mater. Res. **5**, 218–222 (1989)
32. Panitz, J.K.G., Pope, L.E., Lyons, J.E., Staley, D.J.: The tribological properties of MoS_2 coatings in vacuum, low relative humidity, and high relative humidity environments. J. Vac. Sci. Technol. A **6**, 1166–1170 (1988)
33. Zhang, X., Vitchev, R.G., Lauwerens, W., Jiawen, H., Celis, J.P.: Transfer of molybdenum sulphide coating material onto corundum balls. Thin Solid Films **446**, 78–94 (2004)
34. Savan, A., Haefke, H.: MoS_2-based alloys and nanocomposites for solid lubrication. Lubr. Sci. **16**, 229–238 (2004)
35. Singer, I.L., Fayuelle, S., Ehni, P.D.: Wear behavior of triode-sputtered MoS_2 coatings in dry sliding contact with steel and ceramics. Wear **195**, 7–20 (1996)
36. Lieber, C.M., Kim, Y.: Characterization of the structural, electronic and tribological properties of metal dichalcogenides by scanning probe microscopies. Thin Solid Films **206**, 355–359 (1991)
37. Simmonds, M.C., Pflüger, A., Van Swygenhoven, E.: Microstructure and tribological performance of MoS_x/Au co-sputtered composites. J. Vac. Sci. Technol. A **19**, 609–613 (2001)
38. Zhang, X., Lauwerens, W., Jiawen, H., Celis, J.P.: Reorientation of randomly oriented MoS_x coatings during fretting wear tests. Tribol. Lett. **17**, 607–612 (2004)
39. Hu, J.J., Bultman, J.E., Zabinski, J.S.: Microstructure and lubrication mechanism of multilayered MoS_2/Sb_2O_3 thin films. Tribol. Lett. **21**, 169–174 (2006)
40. Zabinski, J.S., Donley, M.S., Walck, S.D., Schneider, T.R., McDevitt, N.T.: The effects of dopants on the chemistry and tribology of sputter-deposited MoS_2 films. Tribol. Trans. **38**, 894–904 (1995)
41. Su, Y.L., Kao, W.H.: Tribological behaviour and wear mechanism of MoS_x–Cr coatings sliding against various counter body. Tribol. Int. **36**, 11–23 (2003)
42. Renevier, N.M., Fox, V.C., Teer, D.G., Hampshire, J.: Coating characteristics and tribological properties of sputter-deposited MoS_2/metal composite coatings deposited by closed field unbalanced magnetron sputter ion plating. Surf. Coat. Technol. **127**, 24–37 (2000)
43. Lince, J.R., Hilton, M.R., Bommannavar, A.S.: Metal incorporation in sputter-deposited MoS_2 films studied by extended X-ray absorption fine structure. J. Mater. Res. **10**, 2091–2105 (1995)
44. Donnet, C., Erdemir, A.: Historical developments and new trends in tribological and solid lubricant coatings. Surf. Coat. Technol. **180–181**, 76–84 (2004)
45. Hilton, M.R., Bauer, R., Didziulis, S.V., Dugger, M.T., Keem, J.M., Scholhamer, J.: Structural and tribological studies of MoS_2 solid lubricant films having tailored metal-multilayer nanostructures. Surf. Coat. Technol. **53**, 12–23 (1992)
46. Zhang, X., Lauwerens, W., Jiawen, H., Celis, J.P.: Structure and growth of basal and random oriented MoS_x coatings deposited by magnetron sputtering. J. Vac. Sci. Technol. **21**, 416–421 (2003)
47. Chen, L.M., Tu, J.P., Zhang, S.C., Peng, S.M., Gu, B.: Effect of deposition pressure on microstructure and tribological behavior of MoS_x/MoS_x-Mo nanoscale multi-layer films. Tribol. Lett. **25**, 87–91 (2007)
48. Voevodin, A.A., O'Neil, J.P., Zabinski, J.S.: WC/DLC/WS2 nanocomposite coatings for aerospace tribology. Tribol. Lett. **6**, 75–78 (1999)
49. Voevodin, A.A., Zabinski, J.S.: Super tough wear-resistant coatings with 'chameleon' surface adaptation. Thin Solid Films **370**, 223–231 (2000)
50. Voevodin, A.A., Zabinski, J.S.: Nanocomposite and nanostructured tribological materials for space applications. Compos. Sci. Technol. **65**, 741–748 (2005)
51. Efeoglu, I.: Co-sputtered Mo:S:C:Ti:B based coating for tribological applications. Surf. Coat. Technol. **200**, 1724–1730 (2005)
52. Fominski, V.Y., Nevolin, R.I., Titov, V.I., Scharff, W.: Tribological properties of pulsed laser deposited WSe_x(Ni)/DLC coatings. Tribol. Lett. **17**, 289–294 (2004)
53. Aouadi, S.M., Paudel, Y., Simonson, W.J., Ge, Q., Kohli, P., Muratore, C., Voevodin, A.A.: Tribological investigation of adaptive MoN_2/MoS_2/Ag coatings with high sulfur content. Surf. Coat. Technol. **203**, 1304–1309 (2009)
54. Savage, R.H.: Graphite lubrication. J. Appl. Phys. **19**, 1–10 (1948)
55. Zabinski, J.S., Bultman, J.E., Sanders, J.H., Hu, J.J.: Multi-environmental lubrication performance and lubrication mechanism of MoS_2/Sb_2O_3/C composite films. Tribol. Lett. **23**, 155–163 (2006)

56. Hamilton, M.A., Alvarez, L.A., Mauntler, N.A., Argibay, N., Colbert, R., Burris, D.L., Muratore, C., Voevodin, A.A., Perry, S.S., Sawyer, W.G.: A possible link between macroscopic wear and temperature dependent friction behaviors of MoS_2 coatings. Tribol. Lett. **32**, 91–98 (2008)
57. Scharf, T.W., Kotula, P.G., Prasad, S.V.: Friction and wear mechanisms in MoS_2/Sb_2O_3/Au nanocomposite coatings. Acta Mater. **58**, 4100–4109 (2010)
58. Krick, B.A., Sawyer, W.G.: Space tribometers: design for exposed experiments on orbit. Tribol. Lett. **41**, 303–311 (2010)
59. Moulder, F., Stickle, W.F., Sobol, P.E., Bomben, K.D: Handbook of X-ray photoelectron spectroscopy, ULVAC-PHI, Inc., Chigasaki, Japan (1995)
60. Carpick, R.W.: The study of contact, adhesion and friction at the atomic scale by atomic force microscopy. Ph.D. Thesis, University of California Berkeley, California (1997)
61. Weber, T., Muijsers, J.C., van Wolput, J.H.M.C., Verhagen, C.P.J., Niemantsverdriet, J.W.: Basic reaction steps in the sulfidation of crystalline MoO_3 to MoS_2, as studied by X-ray photoelectron and infrared emission spectroscopy. J. Phys. Chem. **100**, 14144–14150 (1996)
62. Song, Z., Cai, T., Chang, Z., Liu, G., Rodriguez, J.A., Hrbek, J.: Molecular level study of the formation and the spread of MoO on Au(111) by scanning tunneling microscopy and X-ray photoelectron spectroscopy. J. Am. Chem. Soc. **125**, 8059–8066 (2003)
63. Diaz, J., Paolicelli, G., Ferrer, S., Comin, F.: Separation of the sp^3 and sp^2 components in the C1s photoemission spectra of amorphous carbon films. Phys. Rev. B **54**, 8064–8069 (1996)
64. Balasubramanian, T., Anderson, J.N., Walldén, L.: Surface-bulk core-level splitting in graphite. Phys. Rev. B **64**, 25420 (2001)
65. Raymundo-Piñero, E., Cazorla-Amorós, D., Linares-Solano, A., Find, J., Wild, U., Schlögl, R.: Structural characterization of N-containing activated carbon fibers prepared from a low softening point petroleum pitch and a melamine resin. Carbon **40**, 597–608 (2002)
66. Lizzit, S., Petaccia, L., Goldini, A.: C 1*s* photoemission spectrum in graphite(0001). Phys. Rev. B **76**: 153408-1-4
67. Honma, T., Sato, R., Benino, Y., Komatsu, T., Dimitov, V.: Electronic polarizability, optical basicity and XPS spectra of Sb_2O_3–B_2O_3 glasses. J. Non-Cryst. Solids **272**, 1–13 (2000)
68. Zeng, D.W., Zhu, B.L., Xie, C.S., Song, W.L., Wang, A.H.: Oxygen partial pressure effect on synthesis and characteristics of Sb_2O_3 nanoparticles. Mater. Sci. Eng. A **366**, 332–337 (2004)
69. Chen, X., Wang, X., An, C., Liu, J., Quan, Y.: Synthesis of Sb_2O_3 nanorods under hydrothermal conditions. Mater. Res. Bull. **40**, 469–474 (2005)
70. Torres, J., Alfonso, J.E., López-Carreño, L.D.: XPS and X-ray diffraction characterization of MoO_3 thin films prepared by laser evaporation. Phys. Status Solidi. C **2**, 3726–3729 (2005)
71. Lopez, G.P., Castner, D.G., Ratner, B.D.: XPS O 1*s* binding energies for polymers containing hydroxl, ether, ketone, and ester groups. Surf. Interface. Anal. **17**, 267–272 (1991)
72. Petit, C., Seredych, M., Bandosz, T.J.: Revisiting the chemistry of graphite oxides and its effect on ammonia adsorption. J. Mater. Chem. **19**, 9176–9185 (2009)
73. Dvorak, S.D., Wahl, K.J., Singer, I.L.: In situ analysis of third body contributions to sliding friction of a Pb–Mo–S coating in dry and humid air. Tribol. Lett. **28**, 263–274 (2007)